# Numerical Simulation for a Droplet Fission Process of Electrowetting on Dielectric Device

Dongdong He[1,2], Huaxiong Huang[2,*] and Yongji Tan[1]

[1] *School of Mathematical Sciences, Fudan University, Shanghai, China.*
[2] *Department of Mathematics and Statistics, York University, Toronto, Canada.*

**Abstract.** Electrowetting has been proposed as a technique for manipulating droplets surrounded by air or oil. In this paper, we discuss the modeling and simulation of the droplet fission process between two parallel plates inside an electrowetting on dielectric (EWOD) device. Since the gap between the plates is small, we use the two-phase Hele-Shaw flow as a model. While there are several high order methods around, such as the immersed interface methods [1, 2], we decide to use two first-order methods for simplicity. A ghost-fluid (GF) method is employed to solve the governing equations and a local level set method is used to track the drop interface. For comparison purposes, the same set of two-phase Hele-Shaw equations are also solved directly using the immersed boundary (IB) method. Numerical results are consistent with experimental observations reported in the literature.

**AMS subject classifications**: 76T99, 65M06

**Key words**: Electrowetting, ghost fluid method, Hele-Shaw equations, immersed boundary method, local level set method, microfluidics, moving interface, two-phase flow.

## 1   Introduction

Lab-on-a-chip devices involve miniaturization of many chemical processes onto a single chip. Droplets, as the most common carrier for bio-chemical agents, have been found a growing importance in lab-on-a-chip design. Numerous papers which were centered on droplet operations have been published, c.f. [3–5] and references therein, and droplet-based lab-on-a-chip has been referred to as digital microfluidics. The basic operations include droplet generation; droplet translocation; droplet fusion and droplet fission.

---

*Corresponding author. Email addresses:* `061018014@fudan.edu.cn` (D. He), `hhuang@yorku.ca` (H. Huang), `yjtan@fudan.edu.cn` (Y. Tan)

Amongst the different digital microfluidic systems, electrowetting on dielectric (EWOD) is one of the most promising technique to achieve these goals, because it manipulates discrete droplets rather than a continuous flow.

On the micro-scale, the surface tension forces play a dominate role in the hydrodynamics of a droplet. When a droplet contacts solid electrodes, a wetting force acts on the tri-phase contact line due to electrowetting (changes in the contact angle), and this can be utilized to manipulate the droplet. To avoid electrolysis, an insulating layer is usually inserted between the droplet and electrodes [6–8]. The applications of EWOD devices were discussed extensively in the literature, including microfluid transport [9], tunable optical fiber devices [10], rotating liquid micromotor [11], micro-injection [12], particle separation and concentration control [13]. Other studies focusing on the modeling of EWOD devices can be found in [5,7,14–17].

In this paper we investigate the droplet fission process using a two-phase Hele-Shaw model where the dynamics of both the droplet and the ambient flow is included. We present a ghost fluid (GF) method [19,20] as well as an immersed boundary (IB) method [18] to solve the Hele-Shaw equations. A local level set method [21] is used to track the interface. Our numerical results show that the de-ionized water droplet pinches off without explicit tracking of the interface, contrary to [17] where value of the level set function needs to be artificially reduced to split the droplet.

The rest of the paper is organized as follows. Section 2 explains the basic principle of EWOD and provides a description of the parallel-plate EWOD device and relevant physical parameters. Section 3 presents the Hele-Shaw model for EWOD. Section 4 describes the numerical methods while numerical results are presented in Section 5. Discussion and conclusion are given in Section 6.

## 2   Basic principle of EWOD

It is well known that a droplet on a solid surface spreads or contracts until it has reached the state of minimum free energy, which is determined by cohesive forces in the liquid and the adhesion force between the liquid and the surface. At the tri-phase contact line, the relationship between contact angle $\theta$ and interfacial tensions is given by Young's equation

$$\cos\theta = \frac{\gamma_{SA} - \gamma_{SL}}{\gamma_{LA}}, \tag{2.1}$$

where $\gamma_{SA}$ is the solid-ambient fluid surface tension, $\gamma_{SL}$ is solid-droplet liquid surface tension and $\gamma_{LA}$ is the droplet liquid-ambient fluid interfacial tension.

When an electric voltage is applied, the change of electric charge distribution at the solid-liquid interface alters the free energy on the surface, inducing a change in wettability of the surface and the contact angle of the droplet [22], which is expressed by the

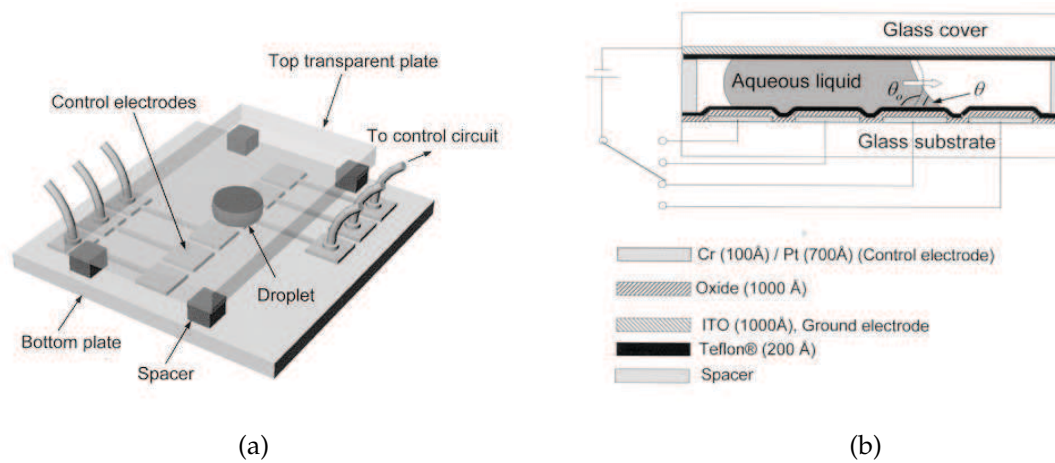(a)                                                                    (b)

Figure 1: (a) Schematic of a parallel-plate EWOD device; (b) Cross-sectional view, reproduced from [5].

Lippmann's equation[†] [23]

$$\gamma_{SL}(V) = \gamma_{SL}(0) - \frac{c}{2}V^2, \tag{2.2}$$

where $c$ is the specific capacitance of the dielectric layer and $V$ is the applied voltage. Combining (2.1) and (2.2) yields the Lippmann-Young equation

$$\cos(\theta_V) = \cos(\theta_0) - \frac{1}{2}\frac{cV^2}{\gamma_{LA}}, \tag{2.3}$$

where $\theta_0$ is the contact angle without voltage while $\theta_V$ is the contact angle with applied voltage $V$. This is known as electrowetting [24]. An insulating layer is usually inserted between the droplet and electrodes to avoid electrolysis.

A schematic of an EWOD device is given in Fig. 1. It consists of a glass cover, a top electrode (transparent plate) with hydrophobic Teflon coating ($\sim$200 Å), spacers on each side of the droplet which assures the gap between the two plates is uniform ($\sim$70$\mu$m), a solid dielectric silicon dioxide ($\sim$1000 Å) with Teflon coating ($\sim$200 Å), control electrodes (bottom plate) and a glass substrate. Three different size of the control electrodes (1.4 mm $\times$ 1.4 mm, 1.0 mm $\times$ 1.0 mm, 0.7 mm $\times$ 0.7 mm) are used in [5]. By adjusting the voltages of the electrodes, the droplets can be moved or split due to the change of wetting property of the two plates. This is the basic principle of the EWOD device.

---

[†]This equation is only valid under low and medium electric potentials. For higher voltages, experiments show that this relation is no longer valid. There exists a critical voltage beyond which the contact angle does not change any more. This is known as the contact angle saturation phenomena [24, 25].

# 3   Mathematical model

We assume that both droplet and ambient fluids are incompressible and their motion is governed by the incompressible Navier-Stokes equations

$$\nabla \cdot \vec{u} = 0, \tag{3.1}$$

$$\rho(\vec{u}_t + \vec{u} \cdot \nabla \vec{u}) = -\nabla p + \mu \Delta \vec{u} \tag{3.2}$$

in $\Omega_+^*$ and $\Omega_-^*$, where $\vec{u} = (u, v, w)$ is the velocity, $p$ is the pressure, $\rho$ and $\mu$ are the density and dynamic viscosity, $\Omega^* = \Omega \times [0, H]$ is the whole domain, $\Omega_+^*$ and $\Omega_-^*$ are the regions of ambient fluid and droplet fluid respectively. Here $\Omega$ is the projection of $\Omega^*$ on to the parallel plates, and H is the gap width between two plates. On the droplet liquid-ambient liquid interface, the jump conditions must be satisfied [26]

$$\left[ \begin{pmatrix} \vec{n} \\ \vec{t_1} \\ \vec{t_2} \end{pmatrix} (pI - \tau)\vec{n} \right] = \begin{pmatrix} \sigma_{LA}\kappa \\ 0 \\ 0 \end{pmatrix}, \tag{3.3}$$

where $\vec{n}$ is unit normal vector, $\vec{t_1}$ and $\vec{t_2}$ are orthogonal unit tangent vectors, $I$ is the identity matrix, $\kappa$ is the local curvature of the interface, $\tau$ is the viscous stress tensor for incompressible flow, $\sigma_{LA}$ is the interfacial tension between droplet fluid and ambient fluid, as stated earlier, and finally $[ \cdot ]$ denotes the jump across the interface.

## 3.1   Hele-Shaw equations

We non-dimensionalize the Navier-Stokes equation based on the following scalings

$$x^* = \frac{x}{L}, \quad y^* = \frac{y}{L}, \quad z^* = \frac{z}{H}, \quad u^* = \frac{u}{U}, \quad v^* = \frac{v}{U}, \quad w^* = \frac{w}{V}, \quad t^* = \frac{t}{\frac{L}{U}}, \quad p^* = \frac{p}{\frac{\mu U L}{H^2}}.$$

Substituting (3.1) into the mass conservation (3.1), we obtain

$$\frac{\partial u^*}{\partial x^*} + \frac{\partial v^*}{\partial y^*} + \frac{VL}{UH}\frac{\partial w^*}{\partial z^*} = 0.$$

Thus $V = \frac{HU}{L} = \lambda U$ with $\lambda = \frac{H}{L}$. Non-dimensionalization for the momentum equations (3.2), yields

$$Re\lambda \left( \frac{\partial u^*}{\partial t^*} + u^*\frac{\partial u^*}{\partial x^*} + v^*\frac{\partial u^*}{\partial y^*} + w^*\frac{\partial u^*}{\partial z^*} \right) = -\frac{\partial p^*}{\partial x^*} + \lambda^2 \left( \frac{\partial^2 u^*}{\partial x^{*2}} + \frac{\partial^2 u^*}{\partial y^{*2}} \right) + \frac{\partial^2 u^*}{\partial z^{*2}},$$

$$Re\lambda \left( \frac{\partial v^*}{\partial t^*} + u^*\frac{\partial v^*}{\partial x^*} + v^*\frac{\partial v^*}{\partial y^*} + w^*\frac{\partial v^*}{\partial z^*} \right) = -\frac{\partial p^*}{\partial y^*} + \lambda^2 \left( \frac{\partial^2 v^*}{\partial x^{*2}} + \frac{\partial^2 v^*}{\partial y^{*2}} \right) + \frac{\partial^2 v^*}{\partial z^{*2}},$$

$$Re\lambda^3 \left( \frac{\partial w^*}{\partial t^*} + u^*\frac{\partial w^*}{\partial x^*} + v^*\frac{\partial w^*}{\partial y^*} + w^*\frac{\partial w^*}{\partial z^*} \right) = -\frac{\partial p^*}{\partial z^*} + \lambda^4 \left( \frac{\partial^2 w^*}{\partial x^{*2}} + \frac{\partial^2 w^*}{\partial y^{*2}} \right) + \lambda^2\frac{\partial^2 w^*}{\partial z^{*2}},$$

where $Re = \rho UL/\mu$ is the Reynolds number.

Since the gap width $H \sim 100\ \mu$m and the length $L \sim 1$mm, we have $\lambda \sim 0.1$. In addition, $Re \sim 0.1$ is small. Dropping the higher order term of $\lambda$ and $Re$ yields (in dimensional form)

$$\frac{\partial u}{\partial x} + \frac{\partial v}{\partial y} + \frac{\partial w}{\partial z} = 0, \tag{3.4}$$

$$\mu \frac{\partial^2 u}{\partial z^2} = \frac{\partial p}{\partial x}, \tag{3.5}$$

$$\mu \frac{\partial^2 v}{\partial z^2} = \frac{\partial p}{\partial y}, \tag{3.6}$$

$$\frac{\partial p}{\partial z} = 0. \tag{3.7}$$

We integrate the above equations in $z$ and apply the no-slip condition[‡] $\vec{u}|_{\partial\Omega^*} = 0$. Since (3.7) implies that $p$ is independent of $z$, integrating Eqs. (3.4)-(3.7) respect to $z$ yields the two-dimensional classical Hele-Shaw equations

$$u = -\frac{H^2}{12\mu} p_x, \tag{3.8}$$

$$v = -\frac{H^2}{12\mu} p_y, \tag{3.9}$$

$$0 = \frac{\partial u}{\partial x} + \frac{\partial v}{\partial y}, \tag{3.10}$$

which are valid both inside and outside the droplet, and the problem is also time dependent so that $u = u(x,y,t)$, $v = v(x,y,t)$, $p = p(x,y,t)$. Meanwhile, the droplet interface is moving with the fluid velocity as following equation.

$$\frac{d\vec{X}(t)}{dt} = \vec{u}(\vec{X}(t)) \quad \text{on } \partial\Omega, \tag{3.11}$$

where $\vec{X}(t) = (x(t),y(t))$ represents the droplet interface.

On the droplet and ambient fluid interface $\Gamma$, we apply the Young-Laplace relation

$$[p] = \sigma_{LA} \kappa, \tag{3.12}$$

where the mean curvature of the interface $\kappa$ is approximated by

$$\kappa = \kappa_{xy} + \kappa_z. \tag{3.13}$$

---

[‡]It is well-known that the no-slip condition leads to an non-integrable singularity in the pressure at the moving contact line. A popular remedy is to use a slip condition and we have also implemented the slip condition. However, our numerical tests show that there is almost no difference between the two formulations for the problem considered in this paper.
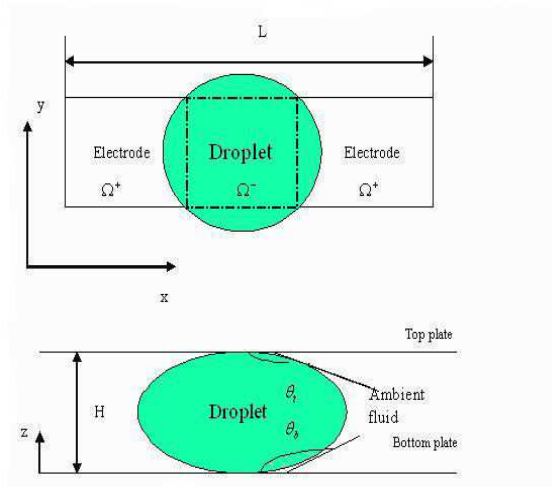
Figure 2: EWOD device geometry. The above figure gives the top view while the bottom figure gives the side view of the EWOD device.

Here $\kappa_{xy}$ represents the curvature on the $xy$ plane (parallel the plates) while $\kappa_z$ represents the curvature of a cross-sectional of the interface along $z$ direction, assuming that it is a circular arc as shown in Fig. 2.

After a simple calculation (see also [17]), we find that

$$\kappa_z = -\frac{\cos(\theta_t) + \cos(\theta_b)}{H}, \tag{3.14}$$

where $\theta_t$ and $\theta_b$ are the contact angles on the top and bottom plates, respectively, c.f. Fig. 2. For the device under consideration, we have $\theta_t = \theta_0$ and $\theta_b$ given by the Lippmann-Young equation (2.3). Our final condition at the interface is given by

$$[\vec{u}] = \left[-\frac{H^2}{12\mu}\nabla p\right] = 0, \tag{3.15}$$

where $\vec{u} = (u, v)$ is the two dimensional velocity vector. And no-penetration boundary condition

$$\vec{u} \cdot \vec{n} = 0, \quad \text{on } \partial\Omega, \tag{3.16}$$

is used here.

## 3.2  Immersed boundary formulation

We can re-cast the set of Hele-Shaw equations with the interface jump conditions into a single set of equations valid in the entire domain, including the interface, using the

immersed boundary formulation

$$\vec{u} = -\frac{H^2}{12\mu}\left(\nabla p - \sigma_{LA}\int_{\Gamma}\kappa\vec{n}\delta(\vec{x}-\vec{x}_{\Gamma})d\vec{x}_{\Gamma}\right), \tag{3.17}$$

$$0 = \nabla\cdot\vec{u}. \tag{3.18}$$

Here $\delta(\vec{x})$ is the Dirac-delta function. Using the signed distance $\phi$ as the level-set function for the interface, we can further simplify the immersed boundary formulation as

$$u = -\frac{H^2}{12\mu}(p_x - \sigma_{LA}\kappa\delta(\phi)n^1), \tag{3.19}$$

$$v = -\frac{H^2}{12\mu}(p_y - \sigma_{LA}\kappa\delta(\phi)n^2), \tag{3.20}$$

$$0 = \frac{\partial u}{\partial x} + \frac{\partial v}{\partial y}, \tag{3.21}$$

where $n^1$ and $n^2$ are the projections of the normal vector $\vec{n}$ on the $x$ and $y$ axes, respectively.

# 4   Numerical methods

In this paper we use two numerical methods to solve the Hele-Shaw equations. In the first approach we use a level-set based GF method by imposing the jump conditions directly. We also implement the IB method based on the immersed boundary formulation for comparison purposes. All the discretizations are based on the nondimensional form of the Hele-Shaw equations using the following scalings

$$x^* = \frac{x}{L}, \quad y^* = \frac{y}{L}, \quad u^* = \frac{u}{U}, \quad v^* = \frac{v}{U}, \quad p^* = \frac{p}{\frac{\sigma_{LA}}{L}}. \tag{4.1}$$

The non-dimensional equations are, after dropping the superscript $*$,

$$\vec{u} = \beta\nabla p, \tag{4.2}$$

$$\nabla\cdot\vec{u} = 0 \tag{4.3}$$

for $\vec{x}$ in $\Omega^+$ and $\Omega^-$ with jump conditions

$$[p] = \kappa_{xy} + \frac{\kappa_z}{\lambda}, \tag{4.4}$$

$$[\vec{u}] = [\beta\nabla p] = 0 \tag{4.5}$$

on $\Gamma$ where

$$\beta = \begin{cases} \beta_+ \triangleq -\dfrac{\lambda^2}{12\eta Ca}, & \vec{x}\in\Omega_+, \\[2mm] \beta_- \triangleq -\dfrac{\lambda^2}{12Ca}, & \vec{x}\in\Omega_-. \end{cases} \tag{4.6}$$

Here $Ca = (\mu_- U)/\sigma_{LA}$ is the capillary number, $\lambda = H/L$ as defined earlier, $\eta = \mu_+/\mu_-$, $\kappa_{xy}$ is the non-dimensional curvature in the $xy$ plane and

$$\kappa_z = -\cos(\theta_t) - \cos(\theta_b). \tag{4.7}$$

In the following, we first describe the discretization, which is followed by a discussion of the local level-set method, the GF method, and finally the IB approach.

## 4.1 Discretization

We use uniform spatial mesh size $\Delta x = \Delta y = h$ in the domain $\Omega$ and $\Delta t$ is the time step. Set $N = 1/\Delta x = 1/\Delta y$ and use $x_i$ to denote the $i$-th point in $x$ direction, $i = 0, \cdots, N$, and $y_j$ and $t_n$ are used in a similar manner. Following [27], we use a staggered grid shown in Fig. 3, with the values of pressure $p$ and level set function $\phi$ stored at the center of each cell while the velocity components $u$ and $v$ stored on the face of the cells. The discretization is done as follows

$$\phi_{i,j}^n = \phi(x_{i-1/2}, y_{j-1/2}, t_n), \quad p_{i,j}^n = p(x_{i-1/2}, y_{j-1/2}, t_n),$$
$$u_{i-1/2,j} = u(x_{i-1}, y_{j-1/2}), \quad u_{i+1/2,j} = u(x_i, y_{j-1/2}),$$
$$v_{i,j-1/2} = v(x_{i-1/2}, y_{j-1}), \quad v_{i,j+1/2} = v(x_{i-1/2}, y_j).$$

Here $x_{i-1/2} = x_i - h/2$ and $y_{j-1/2} = y_j - h/2$ for $i, j = 1, 2, \cdots, N$.

## 4.2 Interface capturing using a local level set method

The level set technique is used to capture the moving interface in this paper. We define the a level set function $\phi$ which takes negative values inside and positive ones outside the droplet and the droplet interface corresponds to the zero level set. The evolution of $\phi$ is given by the transport equation [28]

$$\phi_t + u\phi_x + v\phi_y = 0. \tag{4.8}$$

Initially, the level set function is set to be a signed distance function, cf. Fig. 4(a) on the whole computation domain $\Omega$ defined as

$$\phi(x, y, 0) = \begin{cases} d((x,y), \Gamma(0)), & \text{if } (x,y) \in \Omega^+, \\ 0, & \text{if } (x,y) \in \Gamma(0), \\ -d((x,y), \Gamma(0)), & \text{if } (x,y) \in \Omega^-, \end{cases} \tag{4.9}$$

where $\Gamma(t) = \{(x,y) : \phi((x,y), t) = 0\}$ represents the droplet fluid-ambient fluid interface which is initially a circle on the $xy$ plane in our problem as shown in Fig. 4(b).

Eq. (4.8) is a first-order advection equation. We use a fifth-order upwind HJ WENO scheme [29] to discretize the spatial derivatives, and a third-order TVD Runge-Kutta scheme [30] for the time derivative of $\phi$. However, Eq. (4.8) is not a conservation form,
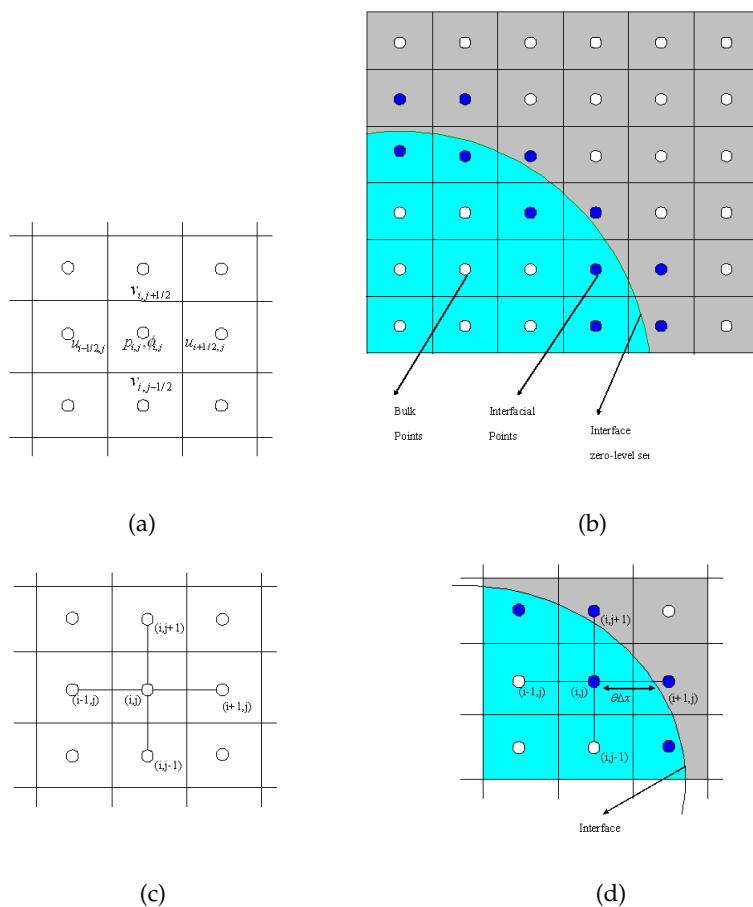
(a)

(b)

(c)

(d)

Figure 3: (a) Schematics of the stagger grids; (b) Definitions of interior and interfacial points. The interface is given by the 0-level set. (c) Standard 5-point stencil for the interior points; (d) The configuration of a typical interfacial point $(i,j)$.
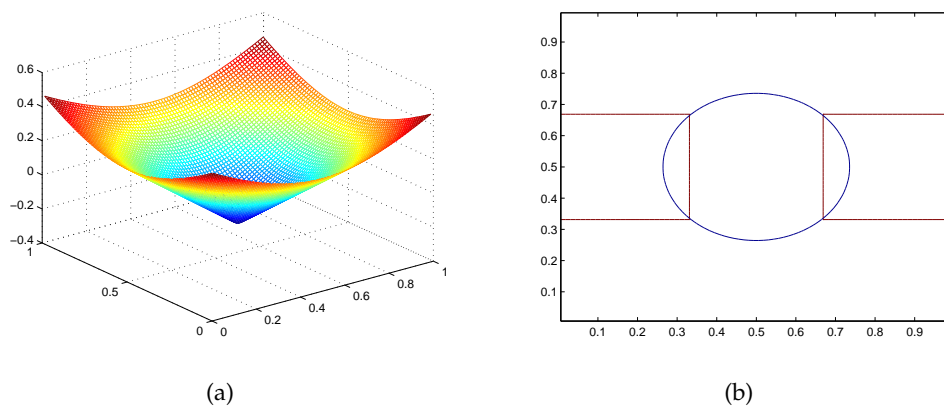


(a)

(b)

Figure 4: (a) Initial level set function; (b) Initial droplet interface.

numerical results show that the mass of the droplet losses (also see [31]). In order to minimize the lose of mass, we combine Eqs. (4.8) and (4.3) together and obtain the following conservation law

$$\phi_t + \nabla \cdot (\vec{u}\phi) = 0. \tag{4.10}$$

In our computation, we also use an upwind HJ WENO scheme to calculate the spatial derivatives of $u\phi$ and $v\phi$ and a third-order TVD Runge-Kutta scheme to calculate the time derivative of $\phi$, results show that the mass loss is reduced.

After applying the evolution equation, the level set function is no longer a signed distance function, one normally needs to reinitialize $\phi$, e.g., using a Hamilton-Jacobi equation

$$\begin{cases} \phi_t + s(\phi)H_G(\phi, \nabla\phi) = 0, \\ \phi(x, y, 0) = \phi_0(x, y), \end{cases} \tag{4.11}$$

with

$$H_G(\nabla\phi) = |\nabla\phi| - 1 \quad \text{and} \quad s(\phi) = \frac{\phi}{\sqrt{\phi^2 + \Delta x^2}}. \tag{4.12}$$

In the computation, $H_G(\nabla\phi)$ is approximated by the Godunov formula [29, 31]

$$
\begin{aligned}
&H_G(\phi_x^+, \phi_x^-, \phi_y^+, \phi_y^-) \\
&= \begin{cases} \sqrt{(\max((\phi_x^+)^-, (\phi_x^-)^+))^2 + (\max((\phi_y^+)^-, (\phi_y^-)^+))^2} - 1, & \text{if } \phi_{i,j} \geq 0, \\ \sqrt{(\max((\phi_x^+)^+, (\phi_x^-)^-))^2 + (\max((\phi_y^+)^+, (\phi_y^-)^-))^2} - 1, & \text{otherwise.} \end{cases}
\end{aligned} \tag{4.13}
$$

Here $(a)^+ = \max(a, 0)$, $(a)^- = -\min(a, 0)$, $\phi_x^+, \phi_x^-, \phi_y^+$ and $\phi_y^-$ are spatial derivatives calculated using the HJ WENO scheme. The reinitialization process is achieved by solving the following equation to steady state

$$\phi_{i,j}^{n+1} = \phi_{i,j}^n - s(\phi_{i,j}^n)\hat{H}_G(\phi_{i,j}^n, \nabla\phi_{i,j}^n)\Delta t. \tag{4.14}$$

The above method is relatively expensive to implement since the reinitialization is done on the entire domain. In order to reduce the computation cost, we use a local level set method [21] in this paper. In all our calculation, we update the level set function in the tube of width $6\Delta x$ around interface and reinitialize the level set function in the tube of width $9\Delta x$. We use reinitialization every 5 time steps, and solve Eq. (4.11) for 100 iterations in each reinitialization.

## 4.3   GF method

We start from the local mass conservation, ie, for each cell $(i, j)$ the local conservation of mass gives

$$\frac{u_{i+1/2, j} - u_{i-1/2, j}}{\triangle x} + \frac{v_{i, j+1/2} - v_{i, j-1/2}}{\triangle y} = 0. \tag{4.15}$$

For interior points, we use the standard central difference to approximate the velocity at each cell face. If $\phi_{i,j} \leq 0$ and $\phi_{i+1,j} \leq 0$, we have

$$u_{i+1/2,j} = \frac{\beta^-(p_{i+1,j} - p_{i,j})}{\Delta x}. \tag{4.16}$$

And if both $\phi_{i,j} > 0$ and $\phi_{i+1,j} > 0$, then

$$u_{i+1/2,j} = \frac{\beta^+(p_{i+1,j} - p_{i,j})}{\Delta x}. \tag{4.17}$$

Velocity $u_{i-1/2,j}$, $v_{i,j+1/2}$ and $v_{i,j-1/2}$ are obtained similarly. Substituting these formulas into (4.15), we obtain the standard five-point difference equation for pressure on cell $(i,j)$, that is for $\phi_{i,j} > 0$,

$$\frac{\beta^+}{\triangle x^2}p_{i-1,j} + \frac{\beta^+}{\triangle x^2}p_{i+1,j} + \frac{\beta^+}{\triangle y^2}p_{i,j-1} + \frac{\beta^+}{\triangle y^2}p_{i,j+1} - \left(\frac{2\beta^+}{\triangle x^2} + \frac{2\beta^+}{\triangle y^2}\right)p_{i,j} = 0 \tag{4.18}$$

and for $\phi_{i,j} \leq 0$,

$$\frac{\beta^-}{\triangle x^2}p_{i-1,j} + \frac{\beta^-}{\triangle x^2}p_{i+1,j} + \frac{\beta^-}{\triangle y^2}p_{i,j-1} + \frac{\beta^-}{\triangle y^2}p_{i,j+1} - \left(\frac{2\beta^-}{\triangle x^2} + \frac{2\beta^-}{\triangle y^2}\right)p_{i,j} = 0. \tag{4.19}$$

For interfacial points, special attention is needed. The key of the GF method is to incorporate the pressure jump condition into the discrete Poisson equation for pressure. On a typical interfacial point $(i,j)$, cf. Fig. 3(d), denote the pressure at the interface and inside the droplet as $p_\Gamma$ and

$$\alpha = \frac{|\phi_{i,j}|}{|\phi_{i,j}| + |\phi_{i+1,j}|}. \tag{4.20}$$

Since $\phi_{i,j} \leq 0$ and $\phi_{i+1,j} > 0$, the jump conditions at the interface (3.15) gives

$$\beta^-\frac{p_\Gamma - p_{i,j}}{\alpha\triangle x} = \beta^+\frac{p_{i+1,j} - (p_\Gamma + [p]_\Gamma)}{(1-\alpha)\triangle x}. \tag{4.21}$$

We obtain $p_\Gamma$ from the above equation as

$$p_\Gamma = \frac{\beta^+\alpha(p_{i+1,j} - [p]_\Gamma) + \beta^-(1-\alpha)p_{i,j}}{\beta^+\alpha + \beta^-(1-\alpha)}. \tag{4.22}$$

From (4.2), we can use the following formula to compute the cell face velocity $u_{i+1/2,j}$:

$$u_{i+1/2,j} = \frac{\beta^-(p_\Gamma - p_{i,j})}{\alpha\Delta x} = \frac{\beta^+\beta^-}{\beta^+\alpha + \beta^-(1-\alpha)}\frac{p_{i+1,j} - p_{i,j} - [p]_\Gamma}{\Delta x}. \tag{4.23}$$

The formula for velocity $u_{i-1/2,j}$, $v_{i,j+1/2}$ and $v_{i,j-1/2}$ are similar and the pressure equation at $(i,j)$ can be obtained by substituting these velocity formulas into (4.15). To find pressure jump $[p]_\Gamma$, we note that

$$[p]_\Gamma = \kappa_{xy} + \frac{\kappa_z}{\lambda} \triangleq a(\vec{x}_\Gamma) \tag{4.24}$$

and approximate $a(\vec{x}_\Gamma)$ by linear interpolation from the value $a_{i,j}$ and $a_{i+1,j}$. More specifically, we use central finite difference method[§] to compute $\kappa_{xy}$, which gives

$$
\begin{aligned}
\kappa_{xy} &= \nabla \cdot \frac{\nabla \phi}{|\nabla \phi|} \\
&= \frac{\phi_x^2 \phi_{yy} - 2\phi_x \phi_y \phi_{xy} + \phi_y^2 \phi_{xx}}{|\nabla \phi|^3} \\
&\approx \frac{(D_x^0 \phi_{i,j})^2 D_y^+ D_y^- \phi_{i,j} - 2 D_x^0 \phi_{i,j} D_y^0 \phi_{i,j} D_y^0 D_x^0 \phi_{i,j} + (D_y^0 \phi_{i,j})^2 D_x^+ D_x^- \phi_{i,j}}{\sqrt{((D_x^0 \phi_{i,j})^2 + (D_y^0 \phi_{i,j})^2)^3}}.
\end{aligned}
\tag{4.25}
$$

To compute $k_z$, we first use the use the contact angle obtained from the Lippmann-Young's equation (2.3) in the region of side electrodes, however, the contact angles in the middle electrode area also change due to the appearance of a varying electric field [6], linear interpretation is used in our computation (more detail will be given in the next section).

Symbolically, we obtain the pressure Poisson equation for cell $(i,j)$

$$
\begin{aligned}
&\frac{\beta_{i-1/2,j}}{h^2} p_{i-1,j} + \frac{\beta_{i+1/2,j}}{h^2} p_{i+1,j} + \frac{\beta_{i,j-1/2}}{h^2} p_{i,j-1} + \frac{\beta_{i,j+1/2}}{h^2} p_{i,j+1} \\
&\quad - \frac{\beta_{i-1/2,j} + \beta_{i+1/2,j} + \beta_{i,j-1/2} + \beta_{i,j+1/2}}{h^2} p_{i,j} = F^x + F^y.
\end{aligned}
\tag{4.26}
$$

A more detailed discussion can be found in [20].

After the pressure is solved with the no-penetration boundary condition (3.16), we can use (4.16), (4.17), and (4.23) to obtain the velocity at cell face. To find velocity $(u,v)$ in the cell center, we use simple averages as

$$u_{i,j} = \frac{u_{i-1/2,j} + u_{i+1/2,j}}{2} \tag{4.27}$$

and

$$v_{i,j} = \frac{v_{i,j-1/2} + v_{i,j+1/2}}{2}. \tag{4.28}$$

These velocity in term will be used in (4.8) to update the level set function.

---

[§]We should point out that we use one-sided finite difference to approximate $\kappa_{xy}$ when the droplet is close to pinch off.

## 4.4 IB method

For numerical calculation based on the immersed boundary formulation, we first regularize the delta function by replacing $\delta(\phi)$ with

$$
\delta_\varepsilon(\phi) = \begin{cases} 0, & \text{if } \phi < -\varepsilon, \\ \dfrac{1}{2\varepsilon} + \dfrac{1}{2\varepsilon}\cos\left(\dfrac{\pi\phi}{\varepsilon}\right), & \text{if } -\varepsilon \le \phi \le \varepsilon, \\ 0, & \text{if } \phi > \varepsilon. \end{cases} \tag{4.29}
$$

We also use the regularized Heaviside function to approximate the viscosity

$$
\mu = \mu_- \left( (1 + (\eta - 1)) H_\varepsilon(\phi) \right), \tag{4.30}
$$

where

$$
H_\varepsilon(\phi)) = \begin{cases} 0, & \text{if } \phi < -\varepsilon, \\ \dfrac{1}{2} + \dfrac{\phi}{2\varepsilon} + \dfrac{1}{2\pi}\sin\left(\dfrac{\pi\phi}{\varepsilon}\right), & \text{if } -\varepsilon \le \phi \le \varepsilon, \\ 1, & \text{if } \phi > \varepsilon. \end{cases} \tag{4.31}
$$

In numerical calculation, we use $\varepsilon = 1.5h$, following [31].

Using Eqs. (4.1) and (3.19)-(3.21), we obtain the non-dimensional equations

$$
\nabla \cdot \vec{u} = 0, \tag{4.32}
$$
$$
\vec{u} = \beta(\phi)(\nabla p - a(x,y)\delta_\varepsilon(\phi)\vec{n}), \tag{4.33}
$$

with

$$
\beta(\phi) = -\frac{\lambda^2}{12(1 + (\eta - 1))H_\varepsilon(\phi)Ca}, \tag{4.34}
$$

$$
a(x,y) = \kappa_{xy} + \frac{\kappa_z}{\lambda}, \tag{4.35}
$$

$$
\vec{n} = \frac{\nabla\phi}{|\nabla\phi|} \triangleq (n^1, n^2). \tag{4.36}
$$

We discretize the equations as

$$
u_{i+1/2,j} = \beta(\phi_{i+1/2,j})\left(\frac{p_{i+1,j} - p_{i,j}}{h} - a_{i+1/2,j}\delta_\varepsilon(\phi_{i+1/2,j})n^1_{i+1/2,j}\right), \tag{4.37}
$$

$$
v_{i,j+1/2} = \beta(\phi_{i,j+1/2})\left(\frac{p_{i,j+1} - p_{i,j}}{h} - a_{i,j+1/2}\delta_\varepsilon(\phi_{i,j+1/2})n^2_{i,j+1/2}\right), \tag{4.38}
$$

where $\delta_\varepsilon(\phi_{i+1/2,j})$ is obtained by (4.29), $\beta(\phi_{i+1/2,j})$ by (4.31) and (4.34), and $n^1_{i+1/2,j}$ by (4.36). To compute $a_{i+1/2,j}$, we simply use interpolation from interpolation from $a_{i,j}$ and

$a_{i+1,j}$, which are the values of $a(\vec{x})$ at cell centers $(i,j)$ and $(i+1,j)$. Similarly, we can calculate $\delta_\varepsilon(\phi_{i,j+1/2})$, $\beta(\phi_{i,j+1/2})$, $n^2_{i,j+1/2}$, and $a_{i,j+1/2}$.

Substitute these equations into (4.15), we obtain the pressure equation on the entire domain

$$
\frac{\beta_{i-1/2,j}}{h^2}p_{i-1,j}+\frac{\beta_{i+1/2,j}}{h^2}p_{i+1,j}+\frac{\beta_{i,j-1/2}}{h^2}p_{i,j-1}+\frac{\beta_{i,j+1/2}}{h^2}p_{i,j+1}
$$
$$
-\frac{\beta_{i-1/2,j}+\beta_{i+1/2,j}+\beta_{i,j-1/2}+\beta_{i,j+1/2}}{h^2}p_{i,j}
$$
$$
=\frac{\beta_{i+1/2,j}}{h}a_{i+1/2,j}\delta_\varepsilon(\phi_{i+1/2,j})n^1_{i+1/2,j}-\frac{\beta_{i-1/2,j}}{h}a_{i-1/2,j}\delta_\varepsilon(\phi_{i-1/2,j})n^1_{i-1/2,j}
$$
$$
+\frac{\beta_{i,j+1/2}}{h}a_{i,j+1/2}\delta_\varepsilon(\phi_{i,j+1/2})n^2_{i,j+1/2}-\frac{\beta_{i,j-1/2}}{h}a_{i,j-1/2}\delta_\varepsilon(\phi_{i,j-1/2})n^2_{i,j-1/2}, \tag{4.39}
$$

where $\beta_{i+1/2,j}$ denotes $\beta(\phi_{i+1/2,j})$.

We obtain the pressure by solving the above linear equation and use (4.37) and (4.38) to find the velocity at cell face, and also (4.27), finally, (4.28) can be used to update the level set function in Eq. (4.8).

## 5   Numerical results

Numerical simulations are carried out for a variety of parameter values using both the GF and IB methods. In the following, we will present two sets of results. In the first set, we compare the results from both methods with the experimental observation in [5] and the parametric study on the effect of viscosity ratio using the GF method is presented in the second set.

### 5.1   Experimental observations and numerical results

Our first set of computations is based on the device used in a sealed air environment [5] where the voltages of the three electrodes from left to the right are 25, 0, 25, respectively. We assume that the air is incompressible so that the two-phase flow model discussed as above can be used. The relevant physical parameters are listed in Table 1. In our computations, we use the $80\times80$ grid and Eq. (4.10) to update the level set function. In addition, we assume that the voltage varies linearly between the electrodes, which is used in Eq. (2.3) to calculate the contact angle. In Fig. 5, the drop splitting process simulated by the IB and GF methods is presented. These results show that the droplet pinches off using both methods, consistent with the experimental observation in Fig. 6.

The total area diagram of both methods is given by Fig. 7, we can see that the IB method loss about 16% of mass while GF method loss about 8% of mass. This may be caused by the numerical error during the reinitialization process, and we refer interested readers to [31,32] for more in-depth discussions.
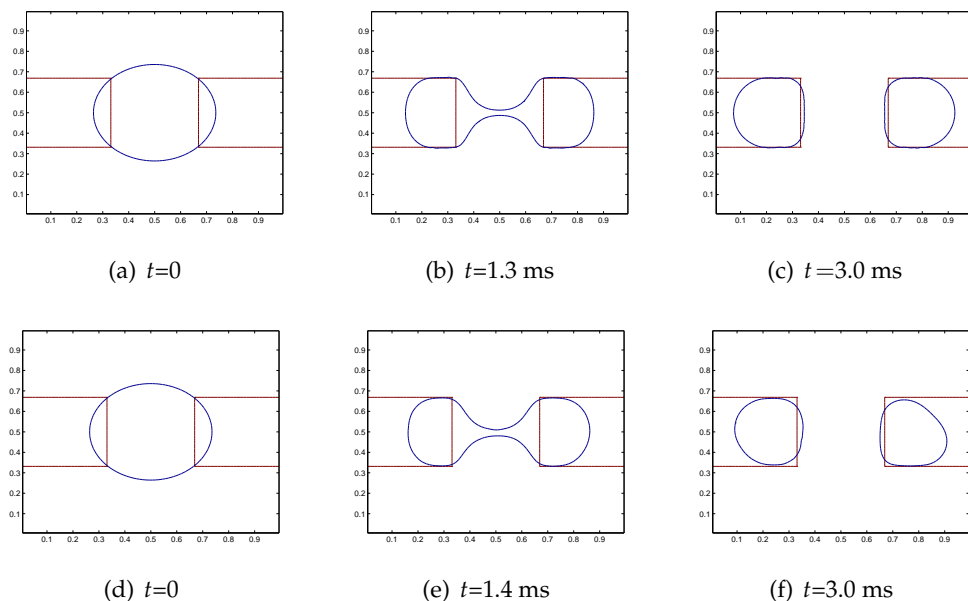
(a) $t$=0                    (b) $t$=1.3 ms                    (c) $t$=3.0 ms

(d) $t$=0                    (e) $t$=1.4 ms                    (f) $t$=3.0 ms

Figure 5: Numerical simulation by GF (a-c) and IB (d-f) methods.



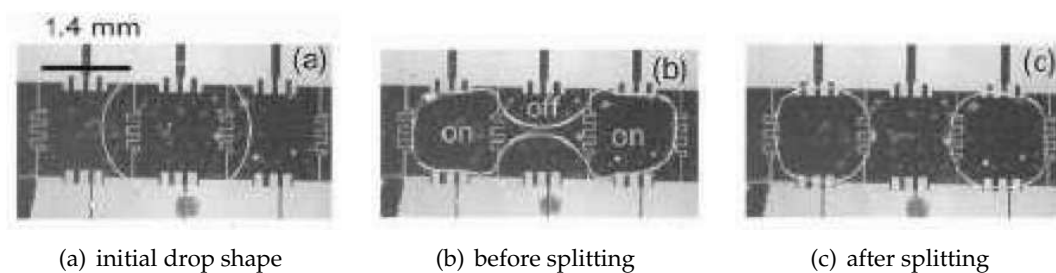(a) initial drop shape        (b) before splitting        (c) after splitting

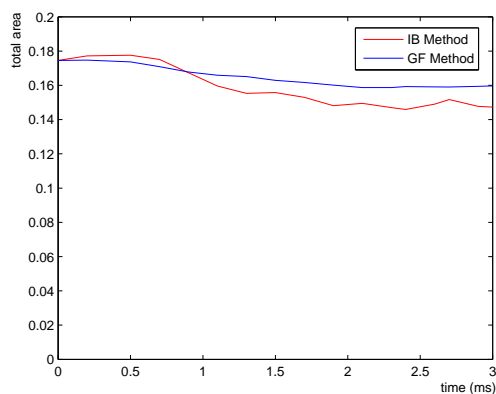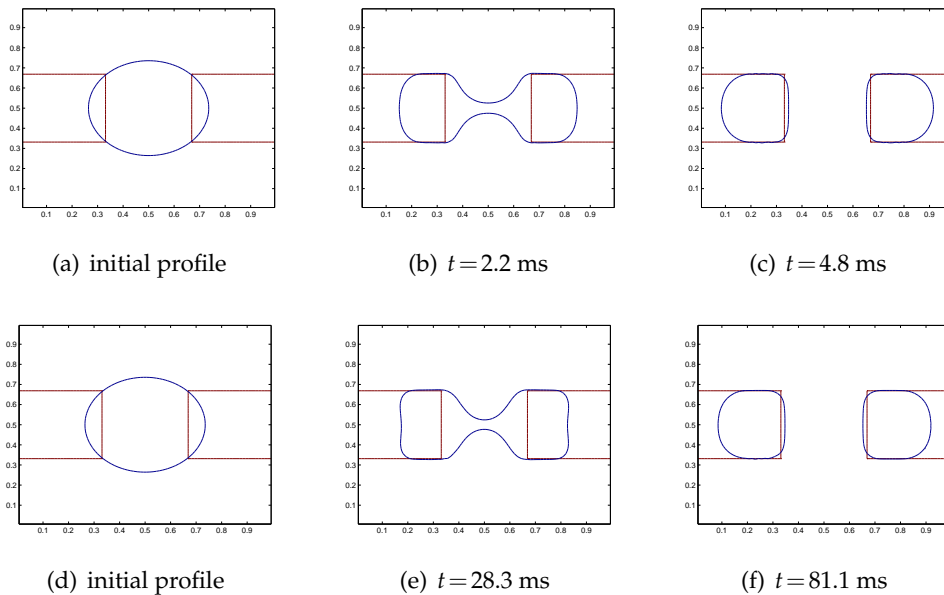Figure 6: Experimental observation of a splitting droplet in EWOD device, reproduced from [5].



Figure 7: Plot of total drop area using IB and GF methods. The exact area is 0.1745.

Table 1: Physical parameter values used in the computation, corresponding to the experiment done in [5].

| Physical Parameters | Values | Units |
|---|---|---|
| Channel Height H | 70 | $\mu$m |
| Electrode Length Scale $L_{eletrode}$ | 1. 4 | mm |
| Computational Domain Length Scale L | 1. 4$\times$3 =4. 2 | mm |
| Dynamic Viscosity Of Air $\mu^+$ | 0.0000183 | Pa$\cdot$s |
| Dynamic Viscosity Of Water $\mu^-$ | 0.00089 | Pa$\cdot$s |
| Interfacial Tension Of Water and Air $\gamma_{LA}$ | 71.99 | mJ/$m^2$ |
| Teflon Layer Height | 200 | Å |
| Dielectric Constant Of Teflon | 2 | |
| Silicon Dioxide Layer Height | 1000 | Å |
| Dielectric Constant Of Silicon Dioxide | 3. 8 | |
| Droplet contact angle in air at zero voltage $\theta_0$ | 117 | ° |
| Applied Voltage | 25 | V |



(a) initial profile　　　　(b) $t=2.2$ ms　　　　(c) $t=4.8$ ms

(d) initial profile　　　　(e) $t=28.3$ ms　　　　(f) $t=81.1$ ms

Figure 8: Numerical simulation by the GF method for $\eta=0.1$ (a-c) and $\eta=10$ (d-f).

## 5.2   Numerical results for different viscosities ratios

In order to demonstrate that the method developed in this paper is capable of capturing the droplet fission process in more general two-phase environments, we provide additional computational results with two different viscosity ratio ($\eta$) values, for $\eta=0.1$ and 10 in Fig. 8.

From these results, we can see that the droplet pinches off for both viscosities ratios. In our calculation, the droplet's splitting time for $\eta=0.1$ is much less than that for $\eta=10$.

Table 2:

| Computational Parameters | Values | Units |
|---|---|---|
| Channel height scale H | 70 | $\mu$m |
| Electrode length scale $L_{eletrode}$ | 1. 4 | mm |
| Applied Voltage | 20 | V |
| Computational domain length scale L | 1. 4$\times$3 =4. 2 | mm |
| Droplet contact angle in ambient environment flow at zero voltage $\theta_0$ | 165 | $^\circ$ |
| Velocity scale $U_0$ | 0.001 | m/s |
| Ratio of the device height and length $\lambda = \frac{H}{L}$ | 0.0167 | |
| Ratio of the viscosity of ambient flow and droplet $\eta$ | I(0.1), II(10) | |
| Capillary Number $Ca$ | 0.00003 | |

Additionally, we found that the droplet's splitting time is strongly correlated to the ratio of the viscosities. This results are consistent with the physical rules as the time scale of the physical problem is determined by capillarity (including wettability) and viscosity.

## 6   Discussion and conclusions

This paper discusses EWOD modeling and simulation based on the two-dimensional two-phase Hele-Shaw equations. The ghost-fluid and immersed boundary methods, coupled with a local level-set method, are employed for comparison purposes. Our results show that both the GF and IB methods are capable of producing numerical results which mimic experimental observations. Our tests also show that the splitting of droplets slows down as the ratio of viscosities the droplets increases, as expected. Our simulations produce a qualitative picture and useful insights into the understanding of the fission process.

We note that both methods suffer loss of mass (area). This could be caused by the reinitialization procedure of the local level-set method, or the discrete error of the GF and IB methods. Reducing mass loss and increasing the accuracy of the methods are the subjects of a future study. Finally, we would like to point out that there are several ways to improve the model used in this study. For example, one could use a more accurate approach to compute the electrical field and related contact angle values by solving a Poisson equation for the electric field. In addition, one can also improve the accuracy by employing the Navier-Stokes equations instead of the Hele-Shaw model.

## Acknowledgments

## References

[1] T. Hou, Z. LI, S. Osher, and H. Zhao, A hybrid method for moving interface problems with application to the Hele-shaw flow. J. Comput. Phys, 134:236–252, 1997.

[2] Z. Li and K. Ito, The Immersed Interface Method: Numerical Solutions of PDEs Involving Interfaces and Irregular Domains. SIAM Frontiers in Applied Mathematics, 33, ISBN-10: 0-89871-609-8 / ISBN-13: 978-0-898716-09-2, 2006.

[3] M.A. Burns, B.N. Johnson, S.N. Brahmasandra, K. Handique, J.R. Webster, M. Krishnan, T.S. Sammarco, P.M. Man, D. Jones, D. Heldsinger, C.H. Mastrangelo, and D.T. Burke, An integrated nanoliter DNA analysis device. Science, 282: 484-487, 1998.

[4] M.G. Pollack, A.D. Shenderov, and R.B. Fair, Electrowetting-based actuation of droplets for integrated microfluidics. Lab Chip, 2: 96-101, 2002.

[5] S.K. Cho, H. Moon and C.-J. Kim, Creating, transporting, cutting, and merging liquid droplets by electrowetting-based actuation for digital microfludic circuits. J.Microelectromechan. Syst, 12(1): 70-80, 2003.

[6] J. Zeng and T. Korsmeyer, Principles of droplet electrohydrodynamics for lab-on-a-chip. Lab Chip, 4: 265-277, 2004.

[7] L.-S. Jang, G.-H. Lin, Y.-L. Lin, C.-Y. Hsu, W.-H. Kan, and C.-H. Chen, Simulation and experimentation of a microfluidic device based on electrowetting on dielectric. Biomed. Microdevices, 9: 777-786, 2007.

[8] L. Minnema, H. A. Barneveld, and P. D. Rinkel, An investigation into the mechanism of water treeing in polyethylene high voltage cables. IEEE Trans. Electr. Insul., EI-15: 461-472, 1980.

[9] W. Satoh, M. Loughran, and F. Mugele, Microfluidic transport based on direct electrowetting. J. Appl. Phys., 96(1): 835-841, 2004.

[10] F. Cattaneo, K. Baldwin, S. Yang, T. Krupenking, S. Ramchandran and J. A. Rogers, Digitally tunable microfluidic optical fiber devices. J. Microlelectromech. Syst. 12(6): 907-912, 2003.

[11] J. Lee, C.-J. Kim, Surface-tension-driven microactuation based on continuous electrowetting. J. Microlelectromech. Syst., 9(2): 171-180, 2000.

[12] K. Hoshino, S.K. Fan, and C.-J. Kim, Enhancement of mixing by droplet-based actuation for mircoinjection. Proc.IEEE Conf.MEMS, Maastricht, The Netherlands, 355-358, 2004.

[13] S.K. Cho, and C.-J. Kim, Particle separation and concentration control for digital microfludic system. Proc. IEEE 16th Annu. Int. Conf. MEMS, Kyoto, Japan, 686-689, 2003.

[14] B. Shapiro, H. Moon, R. Garrell, and C.-J. Kim, Equilibrium behavior of sessile drops under surface tension, applied external fields, and material variations. J. Appl. Phys., vol.93, 2003.

[15] J. Berthier, P. Clementz, O. Raccurt, D. Jary, P. Claustre, C. Peponnet and Y. Fouillet, Computer aided design of an EWOD microdevice. Sensors and Actuators, 127: 283-294, 2006.

[16] H.W. Lu, K. Glasner, A. L. Bertozzi, and C.-J. Kim, A diffuse interface model for eletrowetting droplets in a Hele-Shaw cell. Preprint.

[17] S.W. Walker and B. Shapiro, Modeling the fluid dynamics of Electrowetting on Dielectric (EWOD). J.Microelectromechan. Syst, 15(4): 986-1000, 2006.

[18] M. Sussman, P. Smereka, and S. Osher, A level set method approach for computing solutions to in compressible two-phase flow. J. Comput. Phys., 114: 146-159, 1994.

[19] M. Kang, R. Fedkiw, and X.-D. Liu, A boundary condition capturing method for mutiphase incompressible flow. J. Sci. Comput., 15: 323-360, 2000.

[20] X.-D. Liu, R.P. Fedkiw, and M. Kang, A boundary condtion capturing method for Poisson's Equation on irregular domains. J. Comput. Phys., 160: 151-178, 2000.

[21] D. Peng, B. Merriman, S. Osher, H. Zhao, and M. Kang, A PDE-based fast local level set

method. J. Comput. Phys., 155: 410-438, 1999.

[22]  M. Vallet, B. Berge, and L. Vovelle, Electrowetting of water and aqueous solutions on poly (Ethylene terephthalate) insulating films. Polymer, 37(12): 2465-2470, 1996.

[23]  M.G. Lippmann, Relations entre les phénomènes electriques et capillaires. Ann. Chim. Phys., 5(11): 494-549, 1875.

[24]  H.J.J. Verheijen and M.W.J. Prins,Reversible electrowetting and trapping of charge: model and experiments. Langmuir, 15(20): 6616-6620, 1999.

[25]  M. Vallet and B. Berge, Limiting phenomena for the spreading of water on polymer films by electrowetting. Eur. Phys. J. B, 11: 583-591, 1999.

[26]  L.D. Landau and E.M. Lifshitz, Fluid Mechanics. Pergamon Press, NY, 1978.

[27]  F. Harlow and J. Welch, Numerical calculation of time-dependent viscous incompressible flow of fluid with free surface. Phys Fluids 8, 2182-2189, 1965.

[28]  S. Osher and J.A. Sethian, Front propagating with curvature-dependent speed: algorithms based on Hanilton-Jacobi formulations. J. Comput. Phys., 79(1): 12-49, 1988.

[29]  G. Jiang and D. Peng, Weighted ENO schemes for Halmiton-Jacobi equations. SIAM J. Sci. Comput., 21(6): 2126-2143, 2000.

[30]  C.W. Shu and S. Osher, Efficient implementation of essentially non-oscillatory shock capturing schemes. J. Comput. Phys., 77: 439-471, 1988.

[31]  S. Osher and R. Fedkiw, Level Set Methods and Dynamic Implicit Surface. Springer, NY, 2003.

[32]  M. Sussman and E. Fatemi, An Efficient, Interface-Preserving Level Set Redistancing Algorithm and Its Application to Interfacial Incompressible Fluid Flow. SIAM J. Sci. Comput., 20(4): 1165 - 1191, 1999.

[33]  J. Lee, H. Moon, J. Fowler, C.-J. Kim and T. Schoellhammer, Addressable micro liquid handing by electric control of surface tension. Proc. IEEE Int. Conf. MEMS, Interlaken, Switzerland, 499-502, 2001.